Table 1 Computed natural frequencies

Finite element			Corrected	
14-DOF	3-DOF		3-DOF	
rad/s	rad/s	% error	rad/s	% error
41.74	41.75	0.03	41.74	0.0008
166.99	168.15	0.69	174.77	4.6600
376.16	397.62	5.71	376.15	−0.0030

Table 2 Estimated parameters

	Reduced finite-element model	Correcting term	Corrected model
	$\times 10^5$		
k_{11}	0.28351	−0.01343	0.27008
k_{21}	−0.27119	0.02859	−0.24259
k_{22}	0.39445	−0.04031	0.35414
k_{31}	0.11094	−0.02686	0.08408
k_{32}	−0.27119	0.02859	−0.24259
k_{33}	0.28351	−0.01343	0.27008
	$\times 10^{-1}$		
m_{11}	5.8509	0.01424	5.8651
m_{21}	0.47902	0.02570	0.50472
m_{22}	5.5981	0.04427	5.6423
m_{31}	−0.25279	0.02848	−0.22432
m_{32}	0.47902	0.02570	0.50472
m_{33}	5.8509	0.01424	5.8651

are given in Table 1, and reduced finite-element and corrected parameters are provided in Table 2. It should be noted that the corrected model retains the natural symmetry of the simply supported beam problem (i.e., $k_{11} = k_{33}$, $k_{21} = k_{32}$, $m_{11} = m_{33}$, and $m_{21} = m_{32}$). Figure 2b shows an acceleration spectrum obtained after the load had been moved to one-quarter span.

The corrected model is shown to be significantly more accurate than a Guyan-reduced model in predicting the first and third eigenvalues. In the computation of the second eigenvalue, the reduced model is marginally better than the corrected model. Overall, the corrected model is superior to the reduced model in replicating the measured acceleration spectra. The estimated parameters deviate minimally from the parameters of the initial model and may be considered to be physically meaningful in the sense that a finite-element model is meaningful. As a final test of goodness, the model is able to predict accurately the response of the beam to loading conditions which differ from the loads applied in the test.

Acknowledgment

The author wishes to acknowledge the contribution of C. D. Foster, who conducted the simulated experiment.

References

[1]Berman, A., and Flannelly, W. G., "Theory of Incomplete Models of Dynamic Structures," *AIAA Journal,* Vol. 9, No. 8, 1971, pp. 1481–1487.

[2]Berman, A., "System Identification of Structural Dynamic Models-Theoretical and Practical Bounds," *Proceedings of the AIAA/ASME/ACM/IEEE 25th Structures, Structural Dynamics and Materials Conference,* AIAA, New York, 1984.

[3]Chen, J. C., and Garba, J. A., "Analytical Model Improvement Using Modal Test Results," *AIAA Journal,* Vol. 18, June 1980, pp. 684–690.

[4]Mottershead, J. E., "A Unified Theory of Recursive, Frequency Domain Filters with Application to System Identification in Structural Dynamics," *Transactions of the ASME, Journal of Vibration, Acoustics, Stress and Reliability in Design,* Vol. 110, No. 3, 1988, pp. 360–365.

[5]Mottershead, J. E., Tee, T. K., Foster, C. D., and Stanway, R., "An Experiment to Identify the Structural Dynamics of a Portal Frame," *Transactions of the ASME, Journal of Vibration, Acoustics, Stress and Reliability in Design,* Vol. 112, No. 1, 1990, pp. 78–83.

[6]Stewart, G. W., *Introduction to Matrix Computations,* Academic, New York, 1983.

Effects of Curvature on Composite Material Beams

G. E. Mabson*
Boeing Helicopters, Philadelphia, Pennsylvania

Nomenclature

A'	= laminate A' matrix
a	= constant
b	= flange width
c_1,c_2,c_3,c_4	= constants
D	= laminate D matrix
f	= flange
$FBSC$	= flange bending stiffness coefficient
k_1,k_2,k_3,k_4,k_5	= constants
LC	= lip coefficient
l	= length, l-subscript: lip
M	= laminate moment resultant
N	= laminate stress resultant
NA	= neutral axis
Q	= laminate transverse shear stress resultant
q	= transverse shear loading
R	= radius to flange midplane
$RRSC$	= root radial stiffness coefficient
RS	= radial support
$RTBSC$	= root transverse bending stiffness coefficient
t	= thickness
u	= superscript: undeformed
u,v,w	= displacement in circumferential, y, z or, r directions, respectively
w	= subscript: web
$WPRC$	= web Poisson's ratio coefficient
α	= effectivity
β	= transverse bending factor
ϵ	= strain
σ	= stress

Much of the nomenclature is based on classical lamination theory.[1]

Introduction

CURVATURE can have a significant effect on the stress distributions and failure modes of laminated composite material beams as compared to predicted behavior using isotropic material properties. This Note presents a classical analysis procedure for curved composite material beams with thin flanges.

Curvature effects on beams with wide flanges are illustrated in Fig 1. The major effects of an applied moment in the plane of beam curvature can be summarized as follows.

1) The neutral axis of the beam section shifts toward the concave side.

2) The axial bending stress distribution is nonlinear in the radial direction.

3) The flange axial load induces radial flange loading.

4) The induced radial flange loading causes a transverse flange bending moment and a nonlinear axial bending stress distribution in the flange width direction.

5) The transverse flange bending moment induces interlaminar (radial) stresses in the curved flange root area.

These phenomena (items 1 to 4) have been studied extensively for isotropic materials.[2-4] Design curves are readily

Received June 13, 1989; revision received Aug. 24, 1989.

*Technical Specialist-Stress. Member AIAA.

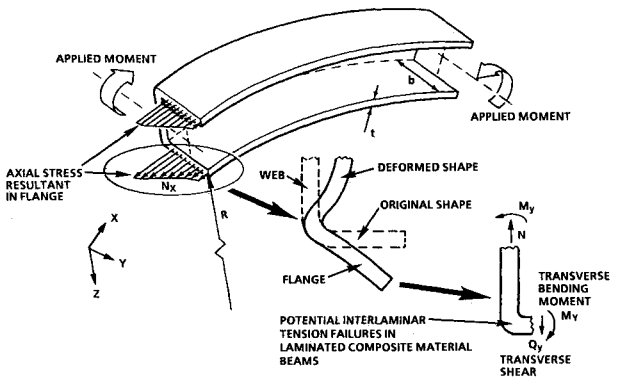

Fig. 1 Curvature effects on beams with wide flanges.

available[5] to allow stress analysts to analyze isotropic beams quickly.

Composite material beams are often designed with their webs optimized for in-plane shear carrying capability and their flanges optimized for in-plane axial loads. This type of design can result in low transverse bending stiffness (i.e., bending stiffness in the plane of the beam cross section) in both the web and the flange, which in turn drastically reduces the flange effectivity and results in transverse bending moments different from predictions for isotropic materials due to increased flange distortions.

Finite element methods have been used to analyze curved composite beams, but these procedures are often unsuitable for initial design purposes.

Flange Stress Analysis

The relationship between the axial flange stress resultant and the flange deflection is (see Fig. 2)

$$N_{x_f} = N^u_{x_f} - \frac{w}{A'_{11_f} R} \tag{1}$$

The transverse bending moment resultant is expressed as

$$M_y = -D_{22_f} \frac{d^2 w}{dy^2} \tag{2}$$

for cylindrical bending about the x axis ignoring in-plane/bending coupling and assuming $t/R \ll 1$. Induced transverse (radial) flange shear loading is related to the transverse bending moment resultant by

$$\frac{d^2 M_y}{dy^2} = -q \tag{3}$$

and also related to the axial flange loading

$$q = \frac{N_{x_f}}{R} \tag{4}$$

Combining Eqs. (1-4) results in

$$\frac{d^4 w}{dy^4} + a^4 w = a^4 A'_{11_f} R N^u_{x_f}$$

where

$$a = \frac{1}{\sqrt[4]{A'_{11_f} D_{22_f} R^2}} \tag{5}$$

The solution is

$$w = -N^u_{x_f} R A'_{11_f} \left[\sin\frac{ay}{\sqrt{2}} \left(c_1 \sinh\frac{ay}{\sqrt{2}} + c_2 \cosh\frac{ay}{\sqrt{2}} \right) + \cos\frac{ay}{\sqrt{2}} \left(c_3 \sinh\frac{ay}{\sqrt{2}} + c_4 \cosh\frac{ay}{\sqrt{2}} \right) - 1 \right] \tag{6}$$

Solution

The four constants (c_1, c_2, c_3, and c_4) are solved for by considering boundary conditions at each end of the flange. Table 1 summarizes the appropriate equations for a flange with a lipped free end. Additional information on the derivation of these equations can be found in Ref. 6.

The distance l_{NA} is measured in the z direction from the flange-root midplane to the location on the web where the slope equals zero. For channel or Z sections, the distance to the neutral axis provides a reasonable estimate. The distance l_{RS} is measured in the z direction from the flange midplane to the location of web radial support (i. e., where the web radial deflection is zero).

Note that the distances l_{NA} and l_{RS} are dependent on the effective section properties, which are values that the analysis is attempting to predict. The initial estimates for these distances are compared to the calculated distances, and an iterative procedure is recommended if there is a significant error. These distances are also dependent on the overall beam boundary conditions. Because of the difficulty in estimating these distances, the use of maximum and minimum possible values may be helpful when attempting to determine conservative predictions.

Flange Stress Ratio

The stress resultant ratio in the flange is

$$\frac{N_x}{N^u_x} = c_1 \sin\frac{ay}{\sqrt{2}} \sinh\frac{ay}{\sqrt{2}} + c_2 \sin\frac{ay}{\sqrt{2}} \cosh\frac{ay}{\sqrt{2}} + c_3 \cos\frac{ay}{\sqrt{2}} \sinh\frac{ay}{\sqrt{2}} + c_4 \cos\frac{ay}{\sqrt{2}} \cosh\frac{ay}{\sqrt{2}} \tag{7}$$

Note that N^u_x is the stress resultant in an undeformed flange (i.e., $w = 0$), not necessarily the stress resultant at $y = 0$ or any other location on the flange.

Flange Effectivity

The flange stress ratio is often difficult to use. A more convenient way of expressing this result is to introduce an "effective flange length" equal to the actual flange length (b) times the flange effectivity (α_f). This effective flange length is the length that would be used when calculating the moment of inertia for overall section bending analysis.

The flange effectivity (α_f) is the ratio of the effective flange cross-sectional area to the actual flange area, and is defined as follows

$$\begin{aligned} \alpha_f &= [(\textstyle\int_0^b N_x \, dy)/N^u_x]/b \\ &= \frac{1}{2k_1} [c_1(\sin k_1 \cosh k_1 - \cos k_1 \sinh k_1) \\ &\quad + c_2(\sin k_1 \sinh k_1 - \cos k_1 \cosh k_1 + 1) \\ &\quad + c_3(\sin k_1 \sinh k_1 + \cos k_1 \cosh k_1 - 1) \\ &\quad + c_4(\sin k_1 \cosh k_1 + \cos k_1 \sinh k_1)] \end{aligned} \tag{8}$$

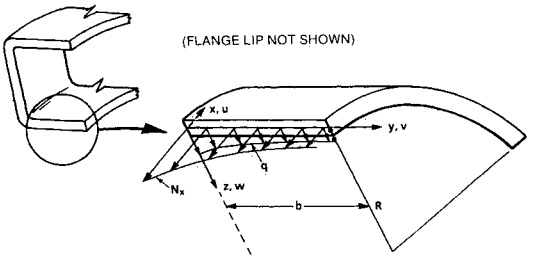

Fig. 2 Flange geometry.

Table 1 Summary of equations for c_1, c_2, c_3, and c_4 for a flange with a lipped free end

$$\begin{bmatrix} \cosh k_1 \cosh k_1 & \cosh k_1 \sinh k_1 & -\sinh k_1 \cosh k_1 & -\sinh k_1 \sinh k_1 \\ \cosh k_1 \sinh k_1 & \cosh k_1 \cosh k_1 & -\cosh k_1 \cosh k_1 & -\cosh k_1 \sinh k_1 \\ -\sinh k_1 \cosh k_1 & -\sinh k_1 \sinh k_1 & -\sinh k_1 \sinh k_1 & -\sinh k_1 \cosh k_1 \\ -k_2 \sinh k_1 \sinh k_1 & -k_2 \sinh k_1 \cosh k_1 & -k_2 \cosh k_1 \sinh k_1 & -k_2 \cosh k_1 \cosh k_1 \\ k_3 & -1 & -1 & 0 \\ 0 & k_4 & -k_4 & -1 \end{bmatrix} \begin{bmatrix} c_1 \\ c_2 \\ c_3 \\ c_4 \end{bmatrix} = \begin{bmatrix} 0 \\ 0 \\ 0 \\ k_5 \end{bmatrix}$$

Note: The fourth equation shown is valid only for $N^u_{x_f} \approx N_{x_f}|_{y=0}$. This can be assumed correct for small radial displacements of the flange/web interface.

Where

$$k_1 = \left(\frac{1}{FBSC}\right)^{0.25} \frac{1}{\sqrt{2}} \left(\frac{b^2}{Rt}\right)^{0.5} = FBSC = \frac{D_{22_f} A'_{11_f}}{t^2}$$

$$k_2 = \frac{LC}{2}\left(\frac{1}{k_1}\right)^3 = LC = \frac{b^3 l_l}{D_{22_f} R^2 A'_{11_l}}$$

$k_3 = 2k_1\ RTBSC = 0$, flange slope = 0 at $y = 0$

$$\begin{cases} = \dfrac{D_{22_f} R}{D_{22_w} b} \ell n \dfrac{R}{R - l_{\mathrm{NA}}}, & \text{channel, outer flange} \\ = -\dfrac{D_{22_f} R}{D_{22_w} b} \ell n \dfrac{R}{R + l_{\mathrm{NA}}}, & \text{channel, inner flange} \\ = \dfrac{D_{22_f} R}{D_{22_w} b}\left[1 + \left(1 - \dfrac{R}{l_{\mathrm{NA}}}\right) \ell n \dfrac{R}{R - l_{\mathrm{NA}}}\right], Z, & \text{outer flange} \\ = -\dfrac{D_{22_f} R}{D_{22_w} b}\left[1 + \left(1 + \dfrac{R}{l_{\mathrm{NA}}}\right) \ell n \dfrac{R}{R + l_{\mathrm{NA}}}\right], Z, & \text{inner flange} \end{cases}$$

$k_4 = k_1^3\ RRSC,$

$$RRSC \begin{cases} = \dfrac{-2D_{22_f} A'_{22_w} R}{b^3} \ell n \dfrac{R}{R - l_{\mathrm{RS}}}, & \text{outer flange} \\ = \dfrac{2D_{22_f} A'_{22_w} R}{b^3} \ell n \dfrac{R}{R + l_{\mathrm{RS}}}, & \text{inner flange} \end{cases}$$

$k_5 = WPRC - 1,$

$$WPRC \begin{cases} = \dfrac{A'_{12_w} l_{\mathrm{RS}}}{A'_{11_w} R}, & \text{outer flange, constant web stress resultant} \\ = \dfrac{-A'_{12_w} l_{\mathrm{RS}}}{A'_{11_w} R}, & \text{inner flange, constant web stress resultant} \\ = \dfrac{A'_{12_w} l_{\mathrm{RS}}}{2A'_{11_w} R}, & \text{outer flange, varying web stress resultant} \\ = \dfrac{-A'_{12_w} l_{\mathrm{RS}}}{2A'_{11_w} R}, & \text{inner flange, varying web stress resultant} \end{cases}$$

Lip Effectivity

The lip effectivity (α_l) is defined similarly to the preceding flange effectivity and is the ratio of the effective lip cross-sectional area to the actual lip area.

$$\alpha_\ell = c_1 \sin k_1 \sinh k_1 + c_2 \sin k_1 \cosh k_1 + c_3 \cos k_1 \sinh k_1 + c_4 \cos k_1 \cosh k_1 \quad (9)$$

Transverse Bending Factor

For isotropic material cross sections, the transverse bending factor (β) is

$$\beta = \sigma_{y\,\mathrm{surface}}/\sigma^u_x$$

For composite material cross sections, the equivalent transverse bending factor is

$$\beta = -6\sqrt{FBSC}c_1 \quad (10)$$

The transverse bending moment resultant at the web/flange interface is

$$M_y\Big|_{y=0} = -\frac{tN^u_x}{6}\beta \quad (11)$$

Summary of Flange Stress Analysis

Bleich's,[2] Anderson's,[3] and Westrup and Silver's[4] "exact" analyses are reproduced by making the following assumptions: 1) isotropic material cross section, 2) rigid webs in transverse bending (or enforcing symmetry about the $y = 0$ plane), and 3) negligible web/flange interface radial displacement.

Radial Stress in the Web/Flange Radius

Beams designed using composite materials often have flange/web interfaces with the laminate curving from the flange to the web with a constant radius.

The transverse bending moment (see Fig. 1) at the flange root causes radial (i.e., interlaminar) stresses at the web/flange radius.

In a curved beam, one source of this transverse bending moment was described [see Eq. (11)].

These radial stresses are much smaller in magnitude than the in-plane stresses for most practical beams. In metal beams, where the material properties are similar in all directions, these radial stresses usually have minimal effects on failures compared to the in-plane stresses. In epoxy matrix composites, these radial stresses can lead to the primary mode of failure. Recently, composite structures have been analyzed for this phenomenon for compressive radial stresses and for tensile radial stresses.[7,8] These analyses rely primarily on finite element techniques that can be too time consuming and cumbersome for initial sizing of structure. A partial closed form solution for a one-ply laminate is presented in Ref. 9. An overview of failures in curved regions of composite hardware due to transverse tensile stresses is presented in Ref. 10.

A classical solution for this phenomenon is presented in Ref. 11. This is an exact closed form analysis of a curved laminate subjected to bending and/or thermal loading and provides an ideal companion to the analysis presented in this paper.

Conclusions

A classical solution for bending in a curved composite beam has been presented. Predicted quantities include flange effi-

ciency factors, transverse bending factors, and in-plane flange stress distributions. The solution presented reproduces previously accepted solutions for isotropic materials when the appropriate assumptions are made. This solution enables curved composite beams with thin flanges to be quickly analyzed.

References

[1]Ashton J. E., Halpin, J. C., and Petit, P. H., *Primer on Composite Materials: Analysis,* Technomic Publishing Co., 1969.

[2]Bleich, H., "Stress Distribution in the Flanges of Curved T and I Beams," U.S. Dept. of the Navy, David W. Taylor Model Basin, transl. 228, 1950.

[3]Anderson, C. G., "Flexural Stresses in Curved Beams of I- and Box-Section," *Proc. Instr. Mech. Engrs.,* Vol. 163, Nov. 1950.

[4]Westrup, R. W., and Silver, P., "Some Effects of Curvature on Frames," *J. Aero/Space Sci.,* Vol. 25, No. 9, Sept. 1958, pp. 567–572.

[5]ESDU 71004, "Flange Efficiency Factors for Curved Beams Under Bending in the Plane of Curvature."

[6]Mabson, G. E., "Effects of Curvature on Composite Material Beams," AIAA Paper 89-1362, April 1989.

[7]Rich, M. J., and Lowry, D. W., "Design Analysis and Test of Composite Curved Frames for Helicopter Fuselage Structure," *AIAA Journal,* 1983; also AIAA Paper 83-1005.

[8]Chang, F., and Springer, G. S., "The Strengths of Fiber Reinforced Composite Bends," *Journal of Composite Materials,* Vol. 20, January 1986.

[9]Lekhnitskii, S. G., *Anisotropic Plates,* Gordon and Breach Science Publishers, 1968.

[10]Kedward, K. T., Wilson, R. S., and Mc Lean, S. K., "Flexure of Simply Curved Composite Shapes," *Composites,* Vol. 20, No. 6, 1989.

[11]Mabson, G. E., and Neall, E. P., III., "Analysis and Testing of Composite Aircraft Frames for Interlaminar Tension Failure," National Specialists' Meeting on Rotary Wing Test Technology of the American Helicopter Society, Bridgeport, CT, March 1988.

Finite Element Analysis of Long Cylindrical Shells

Dan Givoli*

Technion—Israel Institute of Technology, Haifa, Israel

Introduction

THE numerical analysis of long structural elements such as beams and cylindrical shells often requires large computational effort. In many cases, the analyst is only interested in a relatively small region in which most of the physical activity takes place. This region may be characterized by some "irregularities," such as geometrical and material nonlinearities, anisotropy, inhomogeneity and nonuniform loading. However, a standard approach necessitates the discretization of the entire beam or cylinder. Thus, part of the computation is superfluous as far as the analyst is concerned. An example is the stress analysis of a helicopter rotor blade, modeled as a long beam. Most of the blade behaves linearly, but near the root there may be a region of plasticity, large rotations and other sources of nonlinearities.

Moreover, in the bending analysis of a cylindrical shell the response typically has the nature of a boundary layer, outside of which the solution decays quickly. This means that only the segment of the cylinder including this boundary layer has to be taken into account in the numerical scheme. Unfortunately, the analyst has usually only a rough ideas as to where this layer ends, and a superfluous domain has to be included in the computation to insure a conservative analysis. Even if large finite elements are being used in the less interesting region, one must use a transition zone in which the elements are made gradually larger, in order to avoid significant local errors. All of these considerations lead to a discretization with many elements.

In this Note, we consider the problem of a long cylindrical shell loaded axisymmetrically. We show how to eliminate most of the domain in an exact manner, such that the remaining computational domain is small. Thus, only a small domain has to be discretized. Also, the ambiguity related to the length of the boundary layer is totally avoided. The procedure adopted here is similar to the one that has been used in Keller and Givoli[1] for the reduced wave equation and in Givoli[2] for the equations of elastostatics. In Givoli and Keller,[3] the general mathematical features of the method are explained in detail.

Finite Element Formulations

In applying the method to one-dimensional bending problems we consider three different finite element formulations. A discussion on these formulations can be found in Strang and Fix,[4] Carey and Oden,[5] and Hughes.[6]

As an example, we consider a cylindrical shell of length L clamped at both ends and loaded axisymmetrically. We assume that outside a small region near the end $x=L$ the cylinder is linear and uniform. We define the computational domain to be the small interval $[R,L]$, where $x=R$ is a point bounding the nonlinear or nonuniform portion of the cylinder. At the point $x=R$ we shall impose an exact boundary condition. This boundary condition is obtained by solving the problem analytically in the large interval $[0,R]$.

The first formulation that we consider is based on the following statement of the problem:

$$(Etc^2u'')+\frac{Et}{a^2}u=p \qquad R<x<L \tag{1}$$

$$u(L)=u'(L)=0 \tag{2}$$

and the exact boundary condition at $x=R$, which has the form

$$\begin{pmatrix} u'''(R) \\ u''(R) \end{pmatrix} = -\begin{pmatrix} m_{11} & m_{12} \\ m_{21} & m_{22} \end{pmatrix}\begin{pmatrix} u(R) \\ u'(R) \end{pmatrix} \tag{3}$$

Here u is the lateral displacement, E the Young's modulus, p the distributed lateral load, t the cylinder thickness, a the cylinder radius, and c the reduced thickness defined by $c^2=t^2/12\,(1-\nu^2)$ where ν is Poisson's ratio. Since u''' and u'' are force quantities and u and u' are displacement quantities, the matrix $\boldsymbol{m}$ in Eq. (3) is the "edge stiffness matrix" in this case.

The resulting finite element formulation is of a C^1 type, in which the shape functions are required to possess a continuous first derivative. The Hermite cubic shape functions satisfy this requirement. The final linear system of finite element equations is $\boldsymbol{Kd}=\boldsymbol{F}$, where $\boldsymbol{d}$ is the vector of unknowns at the nodes, and the stiffness matrix $\boldsymbol{K}$ can be written as the sum

$$\boldsymbol{K}=\boldsymbol{K}^a+\boldsymbol{K}^b \tag{4}$$

Here $\boldsymbol{K}^b$ is the contribution to the stiffness matrix from the exact boundary conditions [Eq. (3)]. An explicit expression for K^b_{AB} is

$$\begin{pmatrix} K^b_{11} & K^b_{12} \\ K^b_{21} & K^b_{22} \end{pmatrix} = Etc^2|_{x=R}\begin{pmatrix} m_{11} & m_{12} \\ -m_{21} & -m_{22} \end{pmatrix} \tag{5}$$

All other entries in $\boldsymbol{K}^b$ are zero. We see that $m_{12}=-m_{21}$ is a necessary condition to maintain the symmetry of $\boldsymbol{K}$.

Received Oct. 28, 1988; revision received March 10, 1989.

*Lecturer, Department of Aerospace Engineering.